J. Astrophys. Astr. (1986), 7, 171–194

Spectrophotometric Studies of CQ Cephei

B. S. Shylaja *Indian Institute of Astrophysics, Bangalore 560034*

Received 1986 *January* 22; *accepted* 1986 *May* 12

Abstract. Spectrophotometric and spectroscopic observations of CQ Cep—the shortest-period binary with WN component—are presented. Excepting the N v λ4603, the fluxes of all other emission lines show enhancement at minima. They can be explained by the Roche surfaces that take into account the strong wind of the WN7 component. Various radial velocity curves for emission and absorption give different orbital solutions with a general positive shift of γ axes. Although N iv λ4058 represents the true motion of the WN7 component, its flux variations are influenced by geometric effects. There is no signature of the companion. The extent of the atmosphere of CQ Cephei appears larger than in V444Cyg, another eclipsing binary with a Wolf-Rayet component.

Key words: Wolf-Rayet binaries—stars, spectrophotometry—stars, individual

1. Introduction

CQ Cep is an eclipsing binary classified as (WN7 + O) (van der Hucht *et al.* 1981) with a period of 1.64 d. The light curve resembles that of the contact W UMa systems. Broadband photometry in the optical region made by various investigators (see references in Stickland *et al.* 1984) suggests variability of orbital period and of the shape of the light curve.

An interesting finding by Hiltner (1950) was the behaviour of He II λ4686, whose minima occurred at phases 0.25 and 0.75 and the intensities increased at phases 0.0 and 0.5. This behaviour was further investigated by Bappu 1951a, b, 1952) and Bappu & Sinvhal (1955, 1959) who pointed out that other emission lines like He II λ5410 and λ4860 also followed the pattern of λ4686.

Hiltner (1950) attempted to explain the behaviour of the emission line of He II λ4686 by assuming that although the nitrogen lines are produced more or less symmetrically, the He II lines are produced throughout a common envelope surrounding both the stars. Khaliullin (1973) obtained data in four wavelength bands (two emissions and two continua) and attempted to model the variation incorporating an assumed variation of the absorption due to secondary. However, no evidence of such absorptions was found subsequently by Stickland *et al.* (1984), although Niemela (1980) found it for He I λ3888 line.

In a recent study of the variation of the radial velocities and light curves, Leung, Moffat & Seggewiss (1983) arrived at a mass ratio of 0.75 for the components though the radial velocities were disparate. The smaller amplitude of the λ4686 radial-velocity

curve has been related to the ejection of hot λ4686-emitting material with a strong radial velocity component directed towards the observer at phase 0.8.

The most recent and exhaustive study of CQ Cep is by Stickland *et al.* (1984), who analysed the IUE data, UBVJKL photometry as well as the radial-velocity measurements in the optical from Hiltner's (1950) plates. Stickland *et al.* obtained a total of 18 continuum light curves covering the wavelength range 0.13–0.3 μm. Their conclusions may be summarized: (1) The light-curve solutions indicate that half the amplitude of light variation is produced by ellipticity effects and the other half by geometric effects. (2) None of the spectral features is an indicator of the companion's presence or motion. (3) The companion does not modify the overall expected variation of excitation velocity characteristics, and in this respect the combined spectrum resembles any other single WN 7 atmosphere. (4) The luminosity ratio implied by light curves is not consistent with allowable radii and separation values unless their masses and temperatures are considerably raised.

The past investigations provide information on the variations of fluxes in the optical region, as a function of phase, only for continuum at $\lambda\lambda$3550, 5300, 4790, 6300 and the emission lines He II λ4686 and λ6562. Our main interest in observing this system was to obtain light curves in all major emission lines in the optical region systematically. Such data combined with existing spectroscopic information in *UV* and optical is likely to give a better insight and may lead us to unravel at least some of the mysteries of this system. Section 2 gives the details of observations and Section 3 the details of light curves and radial velocities. Section 4 discusses the correlation between light and velocity curves for each line studied. A possible model is discussed in Section 5 in terms of the line variations, light-curve solutions and *IR* and *UV* studies. Finally, in Section 6 the results are compared with another eclipsing system with a Wolf-Rayet component—V444 Cyg.

2. Observations

2.1 *Spectrophotometry*

CQ Cep was observed with the automated spectrum scanner (Bappu 1977) with a 600 lines mm^{-1} grating blazed at 7600 Å, at the Cassegrain focus of the 102 cm reflector of Vainu Bappu Observatory, Kavalur, during 1980–84. The blue region ($\lambda\lambda$3800–5800) was covered in the second order with a channel spacing of 5 Å. The red region ($\lambda\lambda$5800–6800) was covered in the first order with a channel spacing of 10 Å. The exit slit was 40 μm in width which corresponds to a resolution of 10 Å in the second order and 20 Å in the first order. The spectroscopic standards from the lists of Hayes (1970) and Breger (1976) were observed every night to derive the extinction coefficients.

2.2 *Reddening Corrections*

The affiliation of CQ Cep to the Cep OB 1 association has been confirmed by Stickland *et al.* (1984) from the observed strengths of interstellar lines in the *UV* spectrum obtained at high resolution. Thus, CQ Cep is at a distance of more than 3 kpc from us and, therefore, its energy distribution will be affected by interstellar reddening. We

determined the reddening corrections by comparing it with 10 Lac (O7 V)—whose reddening corrections are known (Hua, Woo & Nguyen 1982)—at wavelengths selected so as to be free of emission-line contaminations. Similar corrections have been derived by Kuhi (1966) and Hua, Woo & Nguyen (1982). Stickland *et al.* (1984) derived the reddening corrections from the λ2200 depression, using Seaton's curve for reddening. The dereddened energy distributions are shown in Fig. 1, where samples at three different phases are plotted. It may be seen that our values agree well with Stickland *et al.* (1984).

2.3 *Spectroscopic Studies*

The spectrograms obtained with Mt Wilson 60 inch telescope by late Prof. Bappu in 1951–52 were used in this study. The data consist of (1) the blue spectra on baked IIa-O plates covering $\lambda\lambda$4000–5000 at a dispersion of $\sim$ 75 Å mm^{-1} at λ4340, and (2) the red spectra on 103a-F plates covering $\lambda\lambda$5100–6700 at a dispersion of $\sim$ 160 Å mm^{-1} at λ5500. Relative intensity values of the calibration strips were not available. However, the intensity profiles for a few lines (He II $\lambda\lambda$4686, 4860, 5410, Nv λ4058) were provided by Bappu. Radial velocities were already available for some lines (Bappu & Viswanadham 1977; Giridhar 1978). The lines He II λ4860, λ6562, N III λ4640, N V λ4603 and He I λ5876 and λ4471 were measured afresh. For N V λ4603, it was possible to measure both emission and absorption velocities, whereas for He I λ5876, it was possible to measure only the absorption velocities.

3. Results

3.1 *Light Curves*

From the observed energy distributions at various phases, it was possible to construct the monochromatic light curves, as well as to derive the orbital variations of emission fluxes. Based on broadband photometry from various investigators, Stickland *et al.* (1984) and Walker *et al.* (1983) have analyzed the behaviour of the orbital period over the last few decades. It appears that the period has remained constant during the last 45 years. Khaliullin (1973) derived a mean period combining Hiltner's data with his own, and the ephemeris derived by him is similar to that of Semeniuk (1968). We have adopted the ephemeris

$$T_{\min} = 24432456.668 + 1.641246\ E$$

from Semeniuk (1968) for our studies.

Eight wavelengths were selected to be free of line emission and the light curves were constructed. These are shown in Fig. 2. They all generally resemble the λ5300 light curve of Hiltner.

The photometric errors varied from season to season. In 1982, the error at quadratures and conjunctions never exceeded 0.05 mag. In 1983 and 1984 the errors were slightly higher — 0.06 mag at quadratures and 0.08 mag at conjunction. On some occasions, when the error exceeded 0.1 mag, the observations were not included in the light curve.

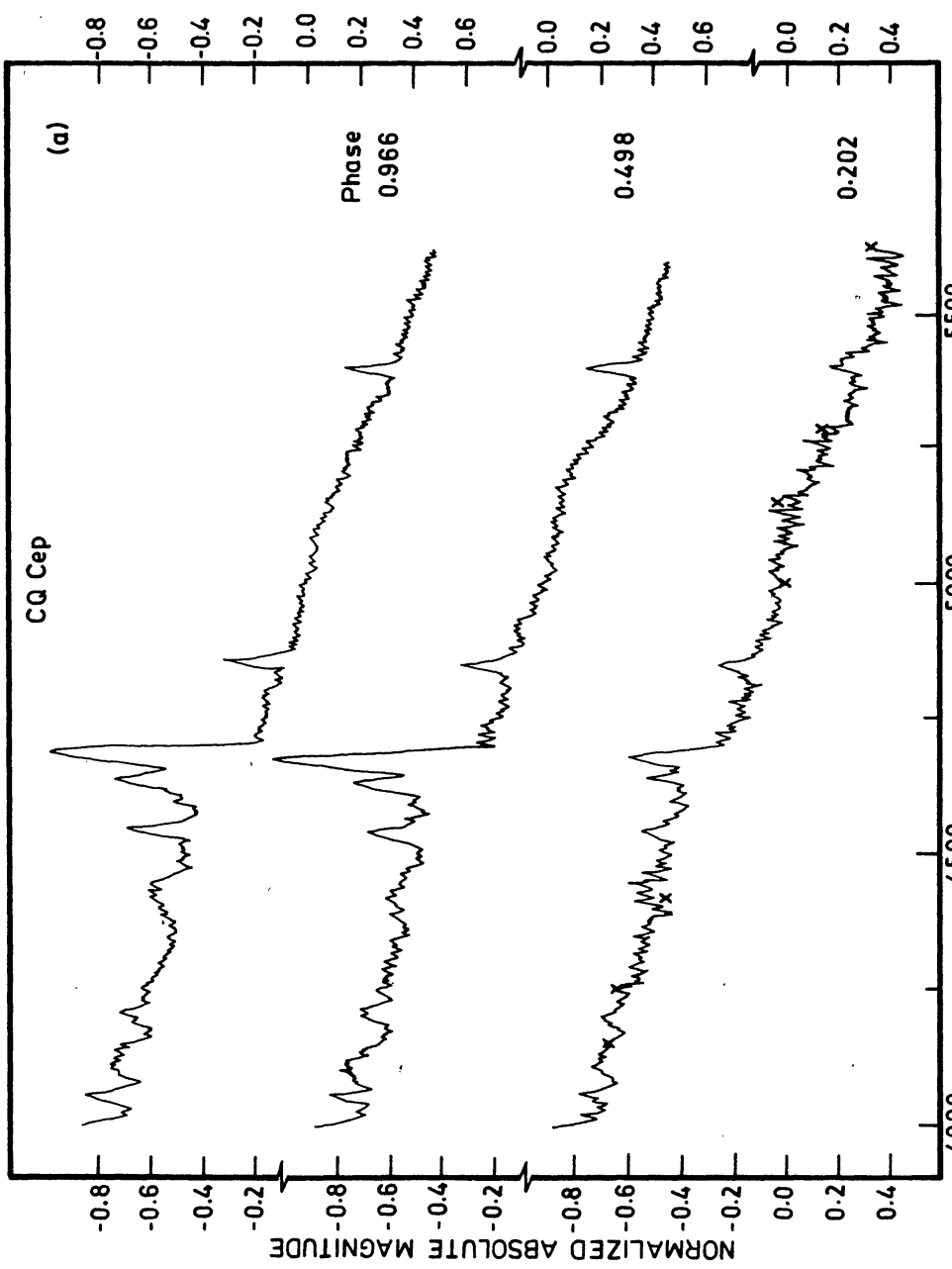

Figure 1. Sample scans of (a) blue region and (b) red region. Crosses correspond to observations of Stickland *et al.* 1984.

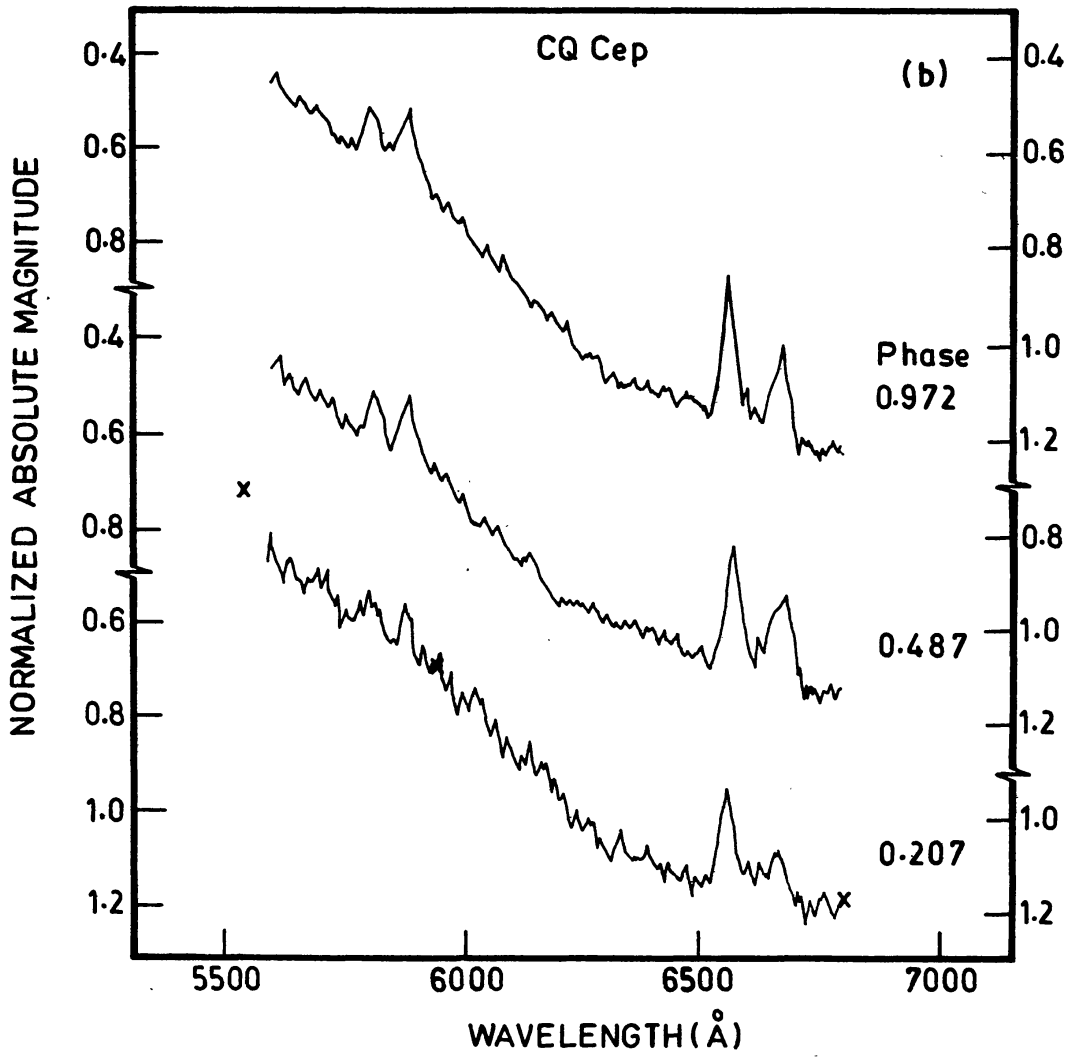

Figure 1. Continued.

3.2 *Emission Line Fluxes*

The fluxes of some lines of He I, He II, N III, N IV, N V and C IV were estimated using the spectrophotometric data. Many lines appear as blends—the most complicated region being λλ4600–4700. N V λ4603 is associated with an absorption throughout the orbit. The emissions of N III λ4640 and He II λ4686 follow immediately and are very strong. In our spectrophotometric scans it was barely possible to resolve these three emissions (at a resolution of 10 Å). The profile was decomposed by hand assuming approximately gaussian components. The continuum was fixed at λλ4460 and 4790. The estimated errors indicated in the flux plots (Figs 3–7) include the errors due to the decomposition procedure as well as the photometric errors. Strong lines like the N IV λ4058 and He II λ4860 have least errors because they are unblended. Intrinsically weak emissions like C IV λ5808 show larger errors.

It was also found that the errors were larger at phases near 0.25 and 0.75. The scan in general looked more noisy probably because the line strengths also diminished at these

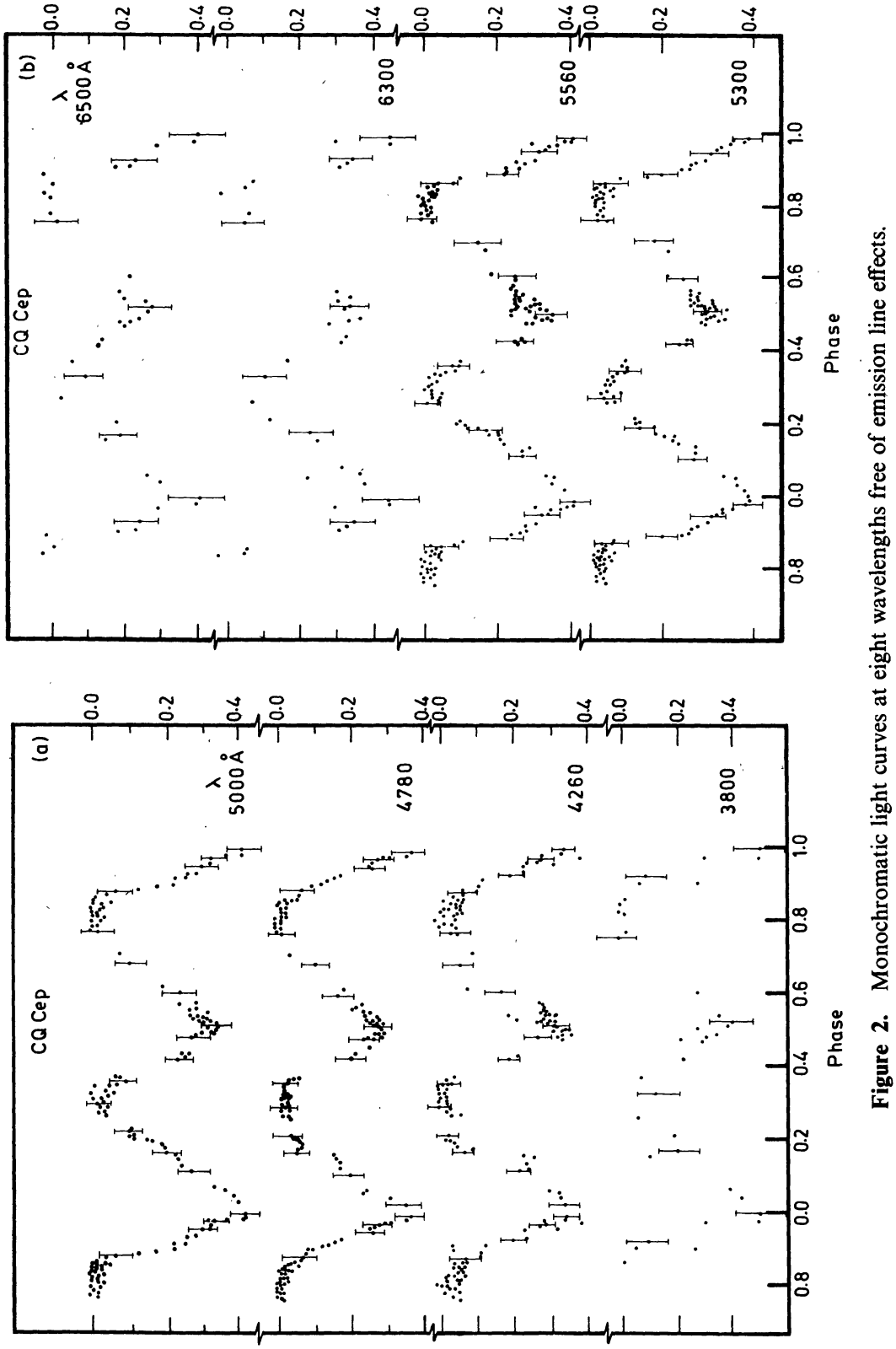

Figure 2. Monochromatic light curves at eight wavelengths free of emission line effects.

phases. At phases close to 0.75 it was not possible to measure the emission fluxes at times because the emission was buried in the continuum noise. Table 1 lists the measured fluxes at different phases.

3.2 *Radial-Velocity Curves*

The radial velocities were measured using the Abbe comparator. The central portion of the emission line was chosen for the measurement. The errors are large (40–60 km s^{-1}) since the features are broad. The radial velocity curves were solved for the orbit by Lehmann-Filhes method. All solutions (including the ones obtained by others) are listed in Table 2. The individual velocity curves appear with the flux plots (Figs 3 to 7). It appears reasonable to assume that the measures of Stickland *et al.* (1984) and Leung, Moffat & Seggewiss (1983) are more accurate by virtue of the method of measurement and solution.

4. Correlation between light and velocity curves

4.1 *Helium lines*

Among the lines of He II studied here ($\lambda\lambda$4686, 4861, 5410, 6562), λ4686 is the strongest. Fig. 3(a) shows the measured line intensities and fluxes, together with the radial velocity measurements of Bappu & Viswanadham (1977), who derived an orbital solution with eccentricity $e = 0.31$ and the velocity for the centre of mass as $\gamma =$ 118 km s^{-1}. Bappu & Viswanadham noted that the line profiles were narrow and sharp at minima and broad and rounded at quadratures. Fig. 3(a) clearly shows the enhancement of flux and intensity near phases 0.0 and 0.5, in conformity with the earlier studies (Hiltner 1950; Khaliullin 1973; Bappu & Viswanadham 1977). The two maxima are of unequal magnitudes, the one closer to phase 0.0 being stronger. Also the maxima appear somewhat earlier than phases 0.0 and 0.5. Similar shift was also noticed by Hiltner (1950), but in the opposite direction. The continuum light curves (Fig. 2) show that the falling edges of the minima are not smooth. Similar effect is probably reflected in the flux measures, as was seen earlier by Walker *et al.* (1983).

The intensities, radial velocities and fluxes of He II λ4860 are shown in Fig. 3(b). Although the behaviour is similar to λ4686 in general, it may be seen that the fluxes at phases 0.0 and 0.5 are of almost similar magnitude and they do not show sudden increase like the latter. Also, the variation is smoother and the fluxes at 0.75 are lower compared to those at 0.25. The amplitude of the radial-velocity curve is slightly larger than that of λ4686 and the orbital solution yields $e = 0.35$ and $\gamma = 196$ km s^{-1}. The line profiles given by Bappu & Viswanadham (1977) show that the violet absorption cuts into the emission wing at some phases especially after the secondary minimum. To study this more clearly, all the plates were checked for the behaviour of this line. It appears that the structure of λ4860 is complex and variable, as noticed by Hiltner (1950). The effect of the absorption on the violet wing is more prominent at phases close to 0.75. There appears to be another absorption component which moves with the emission. Since this component is weak at all phases, it was not possible to measure it precisely.

Table 1. Emission fluxes of CQ Cep.

JD 2440000+	Phase	N IV 4058 $\times 10^{-9}$	N V 4603 10^{-11}	N III 4640 10^{-9}	He II 4686 10^{-9}	He II 4860 10^{-9}	He II 5410 10^{-9}	C IV 5808 10^{-10}	He I 5876 10^{-10}	He II 6562 10^{-10}	He I 6678 10^{-10}	Blend 4100 10^{-9}	Blend 4540 10^{-9}	Blend 4200 10^{-9}
4541.109	0.972	110.0	25.0	204.0	504.0	203.0	133.0	68.0	97.0	182.0	95.0	—	—	—
4542.141	0.601	108.0	72.0	103.0	384.0	103.0	114.0	102.0	180.0	140.0	90.0	—	—	—
5253.180	0.833	68.0	92.0	24.0	571.0	24.0	35.0	18.0	96.0	117.0	62.0	246.0	163.0	114.0
5253.196	0.842	165.0	102.0	58.0	410.0	58.0	—	—	—	—	—	219.0	199.0	184.0
5253.209	0.850	75.0	78.0	88.0	522.0	88.0	—	—	—	—	—	282.0	160.0	93.0
5253.219	0.857	56.0	83.0	127.0	478.0	127.0	—	—	—	—	—	163.0	184.0	59.0
5253.231	0.863	63.0	76.0	84.0	431.0	84.0	—	—	—	—	—	180.0	136.0	84.0
5253.244	0.871	72.0	72.0	87.0	484.0	87.0	—	—	—	—	—	170.0	207.0	63.0
5253.257	0.879	74.0	68.0	75.0	490.0	75.0	—	—	—	—	—	158.0	190.0	110.0
5253.272	0.888	85.0	66.0	74.0	625.0	74.0	—	—	—	—	—	167.0	177.0	148.0
5253.286	0.897	146.0	58.0	77.0	587.0	77.0	—	—	—	—	—	234.0	274.0	79.0
5253.299	0.905	175.0	44.0	147.0	480.0	147.0	92.0	65.0	132.0	190.0	72.0	196.0	153.0	98.0
5254.091	0.917	84.0	53.0	162.0	432.0	162.0	—	—	—	—	—	137.0	140.0	87.0
5254.144	0.420	160.0	78.0	87.0	375.0	87.0	136.0	88.0	99.0	95.0	90.0	275.0	150.0	200.0
5254.158	0.429	208.0	84.0	97.0	470.0	97.0	104.0	102.0	147.0	189.0	119.0	257.0	109.0	158.0
5254.239	0.478	180.0	68.0	106.0	468.0	106.0	127.0	90.0	190.0	219.0	135.0	266.0	179.0	201.0
5254.254	0.487	182.0	42.0	92.0	416.0	92.0	141.0	77.0	175.0	199.0	115.0	256.0	132.0	125.0
5254.272	0.498	180.0	59.0	115.0	407.0	115.0	132.0	—	—	—	—	177.0	176.0	96.0
5256.089	0.526	132.0	75.0	83.0	440.0	83.0	—	—	—	—	—	196.0	230.0	83.0
5268.080	0.911	70.0	42.0	151.0	535.0	151.0	—	92.0	87.0	150.0	75.0	115.0	209.0	52.0
5268.106	0.926	115.0	48.0	158.0	480.0	158.0	106.0	109.0	125.0	205.0	102.0	209.0	239.0	50.0
5269.107	0.537	162.0	80.0	114.0	490.0	114.0	77.0	110.0	185.0	225.0	125.0	286.0	198.0	79.0
5314.096	0.948	124.0	42.0	162.0	428.0	162.0	—	—	—	—	—	163.0	60.0	42.0
5314.106	0.954	72.0	47.0	133.0	323.0	133.0	—	—	—	—	—	202.0	80.0	205.0
5314.116	0.960	94.0	38.0	180.0	487.0	180.0	—	—	—	—	—	192.0	224.0	220.0
5314.125	0.966	98.0	25.0	184.0	416.0	184.0	—	—	—	—	—	134.0	168.0	207.0
5314.135	0.972	140.0	22.0	196.0	402.0	196.0	—	—	—	—	—	150.0	177.0	187.0
5314.147	0.979	132.0	18.0	177.0	410.0	177.0	157.0	122.0	170.0	240.0	135.0	201.0	104.0	187.0
5314.158	0.986	149.0	22.0	170.0	412.0	170.0	147.0	110.0	191.0	235.0	140.0	165.0	94.0	137.0
5649.171	0.107	90.0	62.0	150.0	332.0	50.0	—	—	—	—	—	201.0	134.0	125.0

Table 1. Continued.

JD 2440000+	Phase	N IV 4058 $\times 10^{-9}$	N V 4603 10^{-11}	N III 4640 10^{-9}	He II 4686 10^{-9}	He II 4860 10^{-9}	He II 5410 10^{-9}	C IV 5808 10^{-10}	He I 5876 10^{-10}	He II 6562 10^{-10}	He I 6678 10^{-10}	Blend 4100 10^{-9}	Blend 4540 10^{-9}	Blend 4200 10^{-9}
5649.217	0.135	92.0	72.0	—	330.0	—	—	—	—	—	—	97.0	83.0	106.0
5649.235	0.146	72.0	106.0	—	260.0	—	—	—	—	—	—	102.0	110.0	77.0
5649.254	0.157	113.0	115.0	—	290.0	—	35.0	24.0	82.0	180.0	85.0	102.0	110.0	97.0
5651.071	0.264	70.0	78.0	139.0	320.0	39.0	17.0	37.0	51.0	81.0	52.0	75.9	99.0	62.0
5651.091	0.277	98.0	52.0	125.0	267.0	48.0	27.0	—	—	—	—	50.0	38.0	39.0
5651.100	0.283	68.0	76.0	113.0	335.0	53.0	—	—	—	—	—	68.0	55.0	49.0
5651.120	0.294	82.0	64.0	108.0	296.0	58.0	—	—	—	—	—	101.0	75.0	65.0
5651.129	0.300	92.0	78.0	92.0	252.0	62.0	—	—	—	—	—	92.0	115.0	101.0
5651.139	0.306	65.0	82.0	131.0	277.0	51.0	—	—	—	—	—	106.0	92.0	82.0
5651.149	0.312	81.0	52.0	78.0	311.0	58.0	—	—	—	—	—	76.0	65.0	66.0
5651.158	0.318	115.0	106.0	106.0	340.0	60.0	—	—	—	—	—	96.0	110.0	45.0
5651.168	0.324	65.0	78.0	85.0	357.0	65.0	—	—	—	—	—	87.0	88.0	62.0
5651.194	0.339	95.0	92.0	90.0	290.0	50.0	—	—	—	—	—	90.0	117.0	71.0
5651.203	0.345	126.0	65.0	84.0	326.0	64.0	—	—	—	—	—	128.0	95.0	101.0
5651.213	0.351	103.0	60.0	120.0	300.0	60.0	35.0	—	—	—	—	140.0	140.0	101.0
5651.222	0.357	115.0	72.0	109.0	342.0	109.0	—	—	—	—	—	—	—	—
5651.232	0.363	142.0	114.0	175.0	380.0	115.0	—	—	—	—	—	155.0	170.0	115.0
5651.242	0.369	108.0	82.0	120.0	357.0	120.0	119.0	77.0	123.0	172.0	70.0	—	—	—
5660.093	0.124	80.0	102.0	—	295.0	—	—	—	—	—	—	114.0	106.0	82.0
5660.093	0.762	87.0	91.0	55.0	365.0	55.0	18.0	40.0	85.0	70.0	45.0	69.0	75.0	97.0
5660.102	0.767	74.0	107.0	—	260.0	—	—	—	—	—	—	32.0	44.0	86.0
5660.123	0.780	50.0	88.0	64.0	297.0	64.0	—	—	—	—	—	42.0	49.0	73.0
5660.134	0.787	—	102.0	—	312.0	—	—	—	—	—	—	36.0	38.0	66.0
5660.161	0.803	—	110.0	52.0	300.0	52.0	—	—	—	—	—	—	—	—
5660.171	0.809	48.0	78.0	—	275.0	—	—	—	—	—	—	75.0	66.0	109.0
5660.181	0.815	60.0	103.0	—	372.0	—	—	—	—	—	—	86.0	69.0	85.0
5660.191	0.821	50.0	68.0	—	354.0	—	—	—	—	—	—	92.0	98.0	136.0
5660.202	0.828	55.0	97.0	32.0	302.0	32.0	—	—	—	—	—	—	—	—
5660.212	0.834	75.0	92.0	—	302.0	—	—	—	—	—	—	108.0	103.0	77.0
5660.221	0.840	96.0	75.0	—	296.0	—	—	—	—	—	—	99.0	124.0	118.0

Table 1. Continued.

JD 2440000+	Phase	N IV 4058 $\times 10^{-9}$	N V 4603 10^{-11}	N III 4640 10^{-9}	He II 4686 10^{-9}	He II 4860 10^{-9}	He II 5410 10^{-9}	C IV 5808 10^{-10}	He I 5876 10^{-10}	He II 6562 10^{-10}	He I 6678 10^{-10}	Blend 4100 10^{-9}	Blend 4540 10^{-9}	Blend 4200 10^{-9}
5660.231	0.846	88.0	106.0	28.0	365.0	28.0	22.0	28.0	62.0	68.0	60.0	115.0	110.0	185.0
5676.092	0.510	206.0	68.0	158.0	455.0	148.0	109.0	105.0	198.0	192.0	120.0	211.0	201.0	176.0
5676.104	0.517	173.0	62.0	152.0	407.0	152.0	—	—	—	—	—	—	—	—
5676.114	0.523	154.0	78.0	120.0	350.0	120.0	—	—	—	—	—	—	—	—
5676.124	0.530	192.0	51.0	135.0	422.0	105.0	—	—	—	—	—	231.0	176.0	128.0
5676.135	0.536	180.0	72.0	101.0	464.0	101.0	—	—	—	—	—	—	—	—
5676.146	0.543	193.0	69.0	102.0	401.0	102.0	—	—	—	—	—	—	—	—
5676.156	0.549	190.0	101.0	132.0	355.0	132.0	—	—	—	—	—	—	—	—
5676.166	0.555	180.0	91.0	106.0	388.0	106.0	—	—	—	—	—	210.0	162.0	86.0
5676.176	0.561	146.0	81.0	83.0	418.0	83.0	73.0	125.0	152.0	210.0	105.0	—	—	—
5676.187	0.568	161.0	84.0	94.0	382.0	94.0	—	—	—	—	—	—	—	—
5945.535	0.675	95.0	102.0	—	412.0	—	—	—	—	—	—	41.0	109.0	31.0
5945.585	0.705	122.0	83.0	—	395.0	—	—	—	—	—	—	35.0	70.0	22.0
5963.252	0.476	192.0	42.0	—	434.0	165.0	120.0	121.0	132.0	180.0	117.0	152.0	178.0	126.0
5963.257	0.478	251.0	51.0	158.0	421.0	153.0	—	—	—	—	—	210.0	207.0	185.0
5963.317	0.514	251.0	96.0	147.0	350.0	147.0	—	—	—	—	—	177.0	155.0	214.0
5963.326	0.519	176.0	115.0	52.0	380.0	122.0	—	120.0	187.0	220.0	115.0	245.0	215.0	190.0
5963.339	0.527	205.0	98.0	135.0	325.0	135.0	—	—	—	—	—	—	—	—
5963.352	0.535	193.0	90.0	110.0	360.0	110.0	—	—	—	—	—	—	—	—
5963.360	0.540	220.0	90.0	120.0	385.0	98.0	59.0	120.0	175.0	182.0	110.0	135.0	79.0	58.0
5964.144	0.018	190.0	28.0	95.0	320.0	141.0	62.0	—	—	—	—	212.0	198.0	150.0
5964.176	0.038	178.0	58.0	99.0	380.0	108.0	75.0	99.0	160.0	227.0	122.0	201.0	205.0	188.0
5964.202	0.053	162.0	52.0	102.0	360.0	122.0	102.0	—	—	—	—	—	—	—
5964.211	0.059	195.0	85.0	120.0	375.0	92.0	60.0	90.0	155.0	215.0	104.0	176.0	192.0	140.0
6037.113	0.477	—	—	—	—	—	—	101.0	120.0	207.0	99.0	—	—	—
6047.186	0.610	116.0	68.0	—	388.0	—	—	—	—	—	—	110.0	151.0	60.0
6048.092	0.167	—	—	—	—	—	—	35.0	105.0	152.0	57.0	—	—	—
6048.158	0.207	—	—	—	—	—	—	31.0	80.0	122.0	45.0	—	—	—

Table 2. Orbital solutions from radial velocity curves

Line	γ kms^{-1}	K kms^{-1}	e	ω deg	Ref.
He II 4686	117.5	148.2	0.309	323	1
	133.8	164.0	0.26	356.4	2
He II 4860	196.0 ± 11.4	221.9 ± 12.2	0.35 ± 0.02	286 ± 18	6
	198.2	235.8	0.36		2
He II 5411	176.0	230.1	0.095	335	3
He II 6562	206.0 ± 10.2	212.0 ± 12.8	0.23 ± 0.02	331 ± 18	6
N III 4640	−114.0 ± 8.2	127.8 ± 10.4	0.014 ± 0.011	316 ± 20	6
	−114.3	127.0	0.0		2
N IV 4058	−60.8	312.7	0.035	96.7	1
	−53.4	297.4	0.0		2
	−60	310			4
	−85	285			5
N V 4603 em	159.6 ± 7.2	286.0 ± 6.4	0.041 ± 0.017	295 ± 17	6
	153	280			4
N V 4603 abs	−216.1 ± 5.8	307.5 ± 7.3	0.035 ± 0.018	298 ± 18	6
	−220	299			4

References
1. Bappu & Viswanadham (1977).
2. Stickland *et al.* (1984).
3. Giridhar (1978).
4. Leung Moffat & Seggewiss (1983).
5. Niemela (1980).
6. This work.

Fig. 3(c) shows the fluxes and intensities of He II λ5410, and also radial velocities from Giridhar (1978). The orbital solution of Giridhar yields $e = 0.1$ and $\gamma = 176$ km s^{-1}. Giridhar found the line profiles to be generally symmetrical, with an indication of a violet absorption edge after the secondary minimum. The enhancement of flux close to phases 0.0 and 0.5 is smooth, as are the intensity measures.

The radial velocities and flux measurements of He II λ6562 are shown in Fig. 3(d). The orbital solution yields $e = 0.23$ and $\gamma = 206$ km s^{-1}. The density tracings of this region of some spectra are shown in Fig. 4(a), which clearly show the variation of the structure of the line. Like λ4860, this also shows violet absorption effects soon after the secondary minimum. Such an effect appears to be present soon after primary minimum also, but data with better resolution are needed to ascertain this.

Among the He I lines, it was possible to study λ5876 and λ6678. Fig. 4(a) includes the λ6678 region as well. It may be seen that the line profile varies throughout the cycle, making the radial velocity measurements very difficult. Sometimes it appears as though the line is split into two components. Fig. 4(b) shows the structure of λ5876 line. It may be noticed that the violet absorption edge is very strong and appears throughout the orbital cycle, whereas the emissions are not very sharp. Thus it was possible to measure only the absorption velocities. The radial velocity curve shows a large scatter making it difficult to find any orbital solution. The behaviour of flux measures is similar to the other helium lines, but with a smaller amplitude of variations.

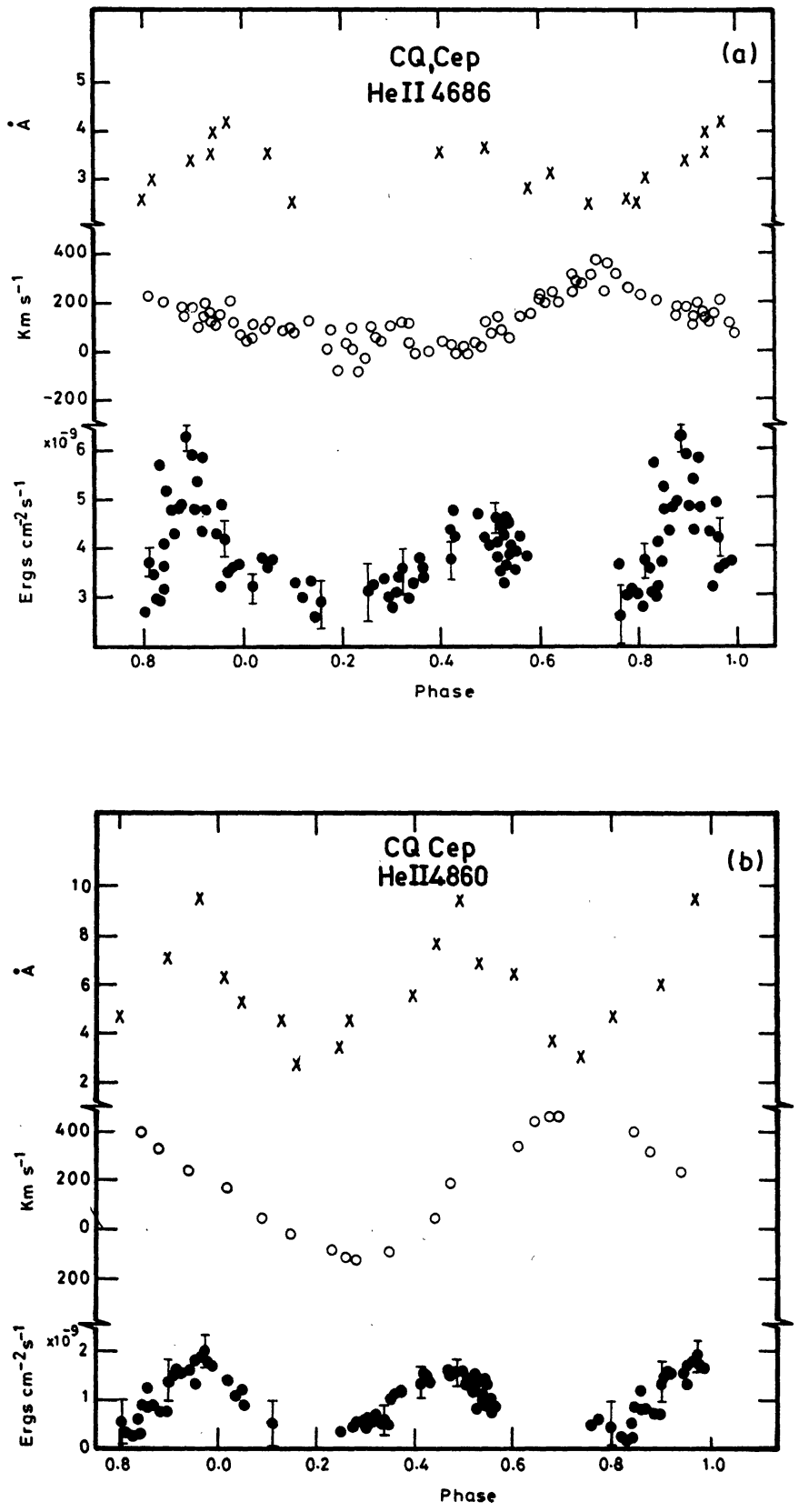

Figure 3. Measured intensities (×), radial velocities O and fluxes ● of He II lines: (a) λ4686, (b) λ4860, (c) λ5410, and (d) λ6562.

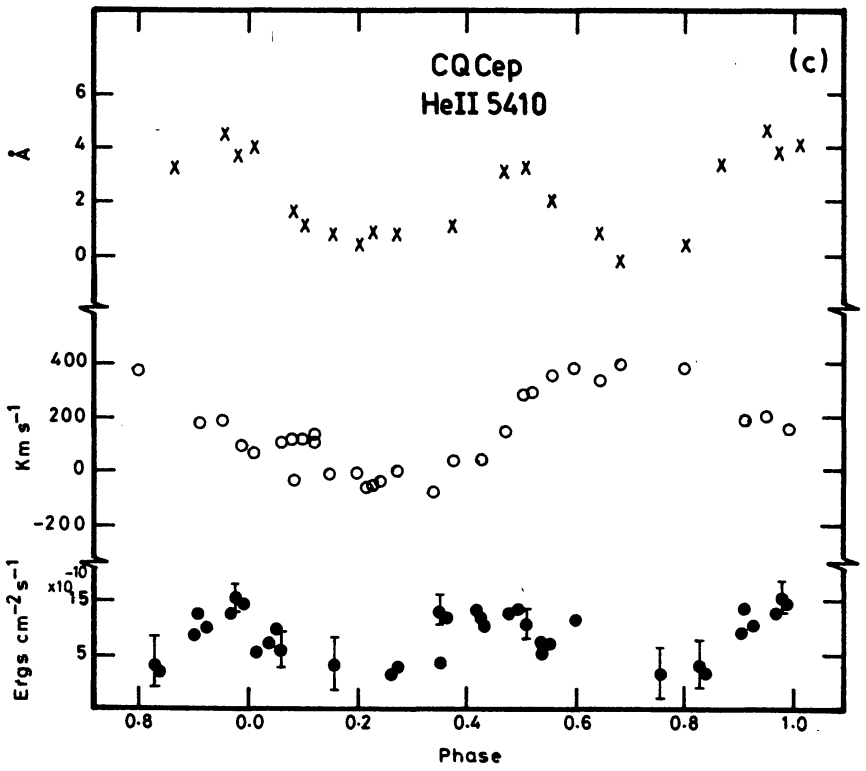

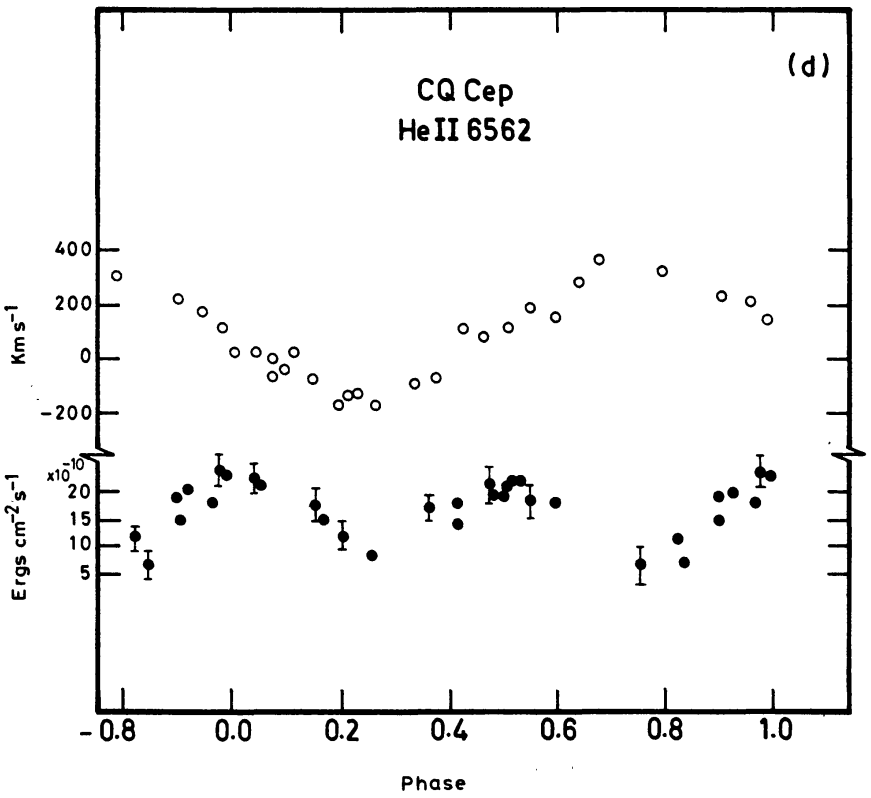

Figure 3. Continued.

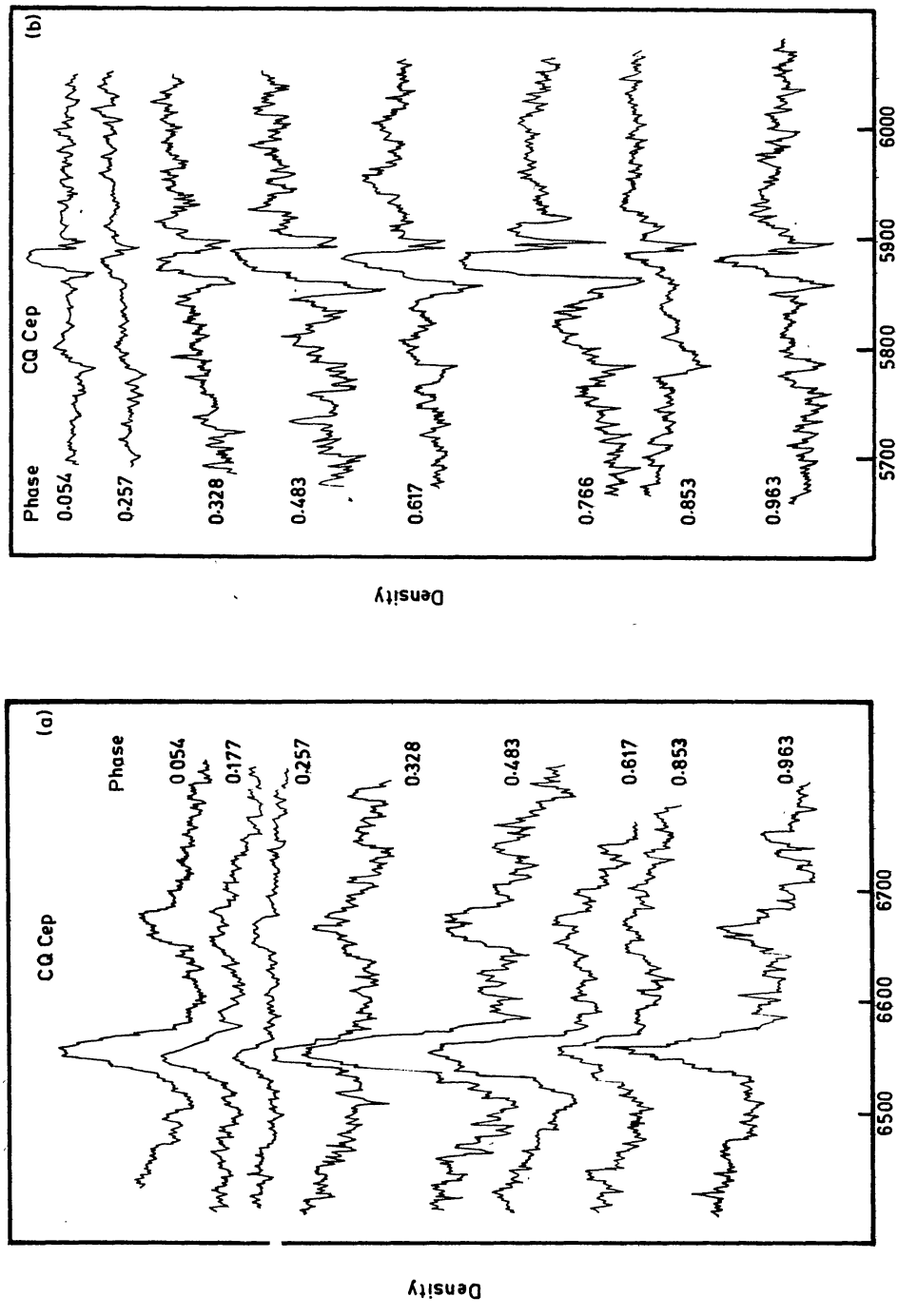

Figure 4. Density tracings at various phases showing the variation in the structure of (a) He II λ6562 and He I λ6678, and (b) He I λ5876.

4.2 *Nitrogen Lines*

The nitrogen lines that are studied are N III λ4640, N IV λ4058, and N V λ4603. The N III line at λ4640 is affected at both the wings by He II λ4686 and N V λ4603. Thus the estimated flux is not expected to be very accurate. Allowing for these errors in flux measures, it may be seen from Fig. 5 that the flux increases at phases 0.0 and 0.5 and the total amplitude of variation is small. Bappu (1973), based on high dispersion spectral studies, has pointed out that this broad emission is probably a blend of more than 3 lines. The radial velocities shown in Fig. 5 were measured for a mean centre of the emission. It appears that the amplitude is quite small compared to radial velocity curves of other lines. An orbital solution gives almost circular orbit with $e = 0.014$ and $\gamma = -114\ \mathrm{km\,s^{-1}}$. It may be noticed that this γ value is different compared to other emission lines.

Bappu & Viswanadham (1977) emphasized that N IV λ4058 is the only line that predicts the true motion of the WN component. They derived the orbital solution with $e = 0.1$ and $\gamma = -62\ \mathrm{km\,s^{-1}}$. They have shown that the profile is not affected by absorptions and is generally symmetrical. Fig. 6 shows the measured line fluxes and intensities, showing enhancement at minima.

Now we turn to N V λ4603, which has a stable profile and exhibits a violet absorption through the orbital phase. It was possible to derive the radial velocity curves for both emission and absorption components. These curves and the flux measures are shown in Fig. 7. The flux measures are probably affected by the violet wing of strong N III line at λ4640, but only high dispersion spectra can ascertain this. The line fluxes above the continuum only are measured, and unlike the variation of other emissions

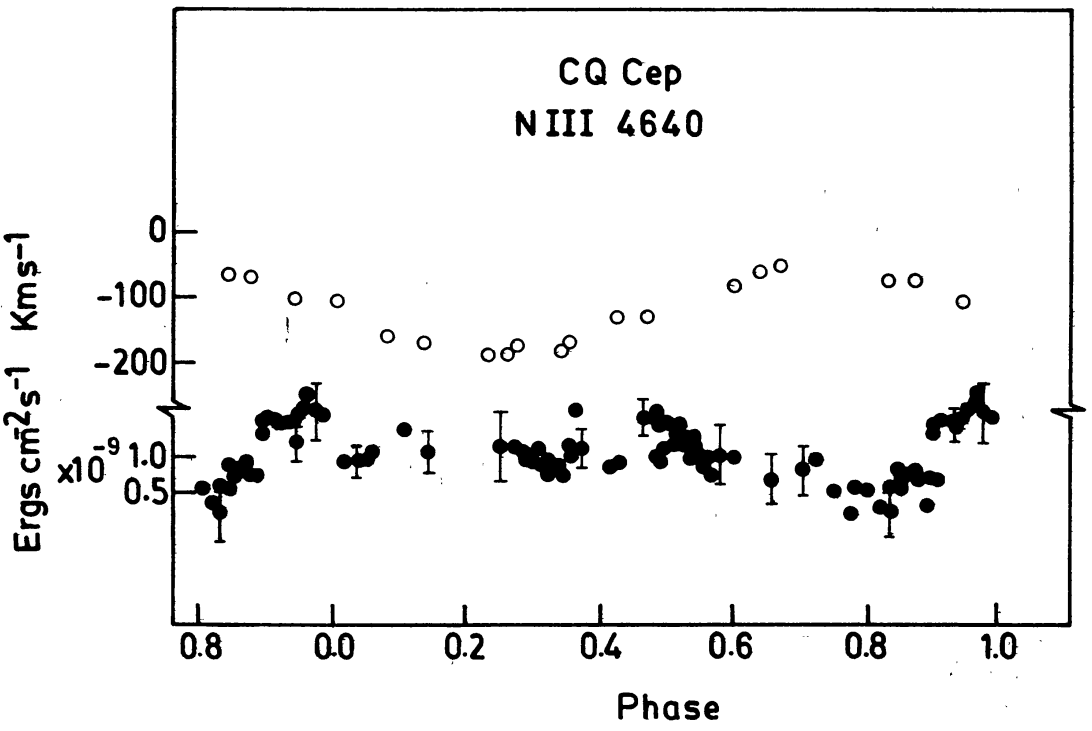

Figure 5. Radial velocity and flux measures of N III λ4640.

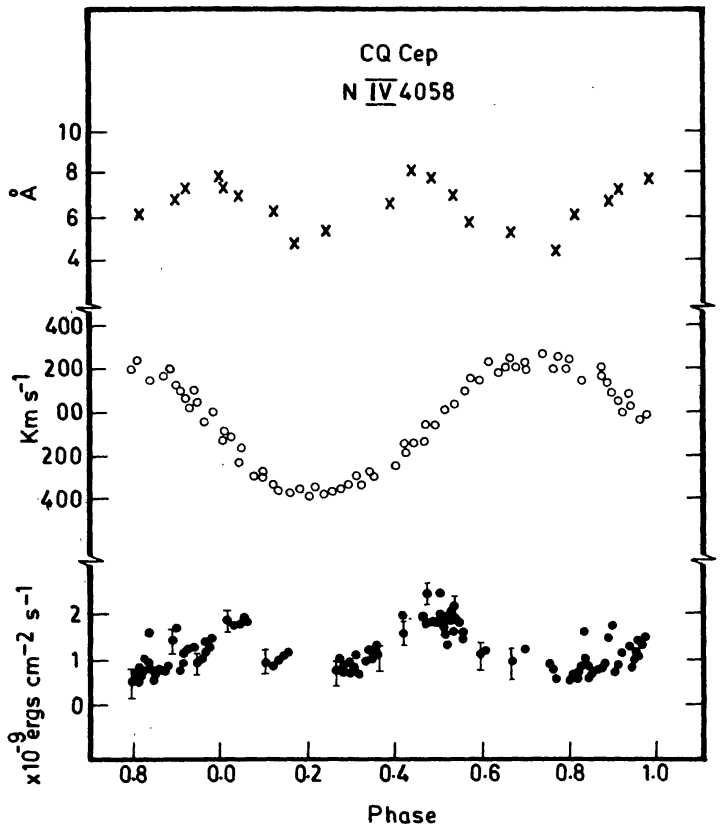

Figure 6. Intensities, radial velocities and flux measures of N IV λ4058.

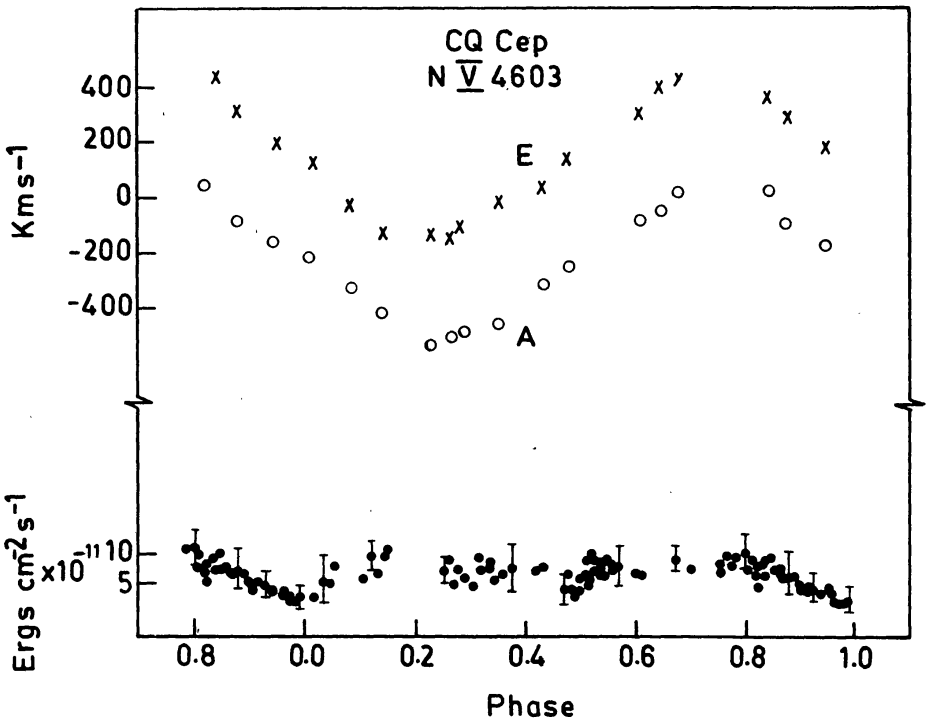

Figure 7. Radial velocity curves for both emission and absorption components, and flux measures of N V λ4603.

discussed till now, these measures show a small dip at phase 0.0. But for this the fluxes are generally constant. Both absorption and emission components give almost circular orbit solutions with only the γ values shifted (Table 2).

4.3 *Carbon Lines*

The only carbon line that was available for measurement of fluxes in our scans is C IV λ5808. The measured fluxes clearly show the same pattern as in the remaining lines. The amplitude of variation is not very large. This region is covered in the density tracings shown in Fig. 4(b), which clearly points out the difficulty in measuring radial velocity, at any phase. Since the spectrophotometric observations made in the red region were not as frequent as in the blue region, the number of flux measures are relatively smaller. This is true also for the other lines in this region *viz.* He I $\lambda\lambda$5876, 6678, and He II λ6562.

4.4 *Line Blends*

We now look at the line blends at $\lambda\lambda$4540, 4200 and 4100. The main contributors to these emissions are known to be He II and N III. These flux measurements show a variation similar to that of other He II lines, indicating that both contributors to these blends behave in the same way. It is difficult to study the behaviour of individual contributors to these blends because of insufficient resolution.

5. Model

All the solutions from different emission-line radial-velocity curves (Table 2), together with the light curve solutions of Stickland *et al.* (1984) and Leung, Moffat & Seggewiss (1983), can be made use of in an attempt to construct a model for CQ Cep.

5.1 *Light Curve Solutions and the Nature of the Companion*

Leung, Moffat & Seggewiss (1983) solved, by Wilson-Devinney method the light curve obtained by Hiltner (1950) at λ5300. They discuss the choice of the mass ratio 0.75 in a great detail. Stickland *et al.* (1984) solved the same light curve taking into account the atmospheric eclipses, and arrived at a mass ratio of 0.6. Both the solutions necessitate a massive companion of the order of 35–38 $M_\odot$. The mass of WN component—46 $M_\odot$ from Leung, Moffat & Seggewiss (1983) and 64 $M_\odot$ from Stickland *et al.* (1984)—appears large compared to other estimates for WN components in binaries: 10 $M_\odot$ for V444 Cyg (Kuhi 1968), 5–12 $M_\odot$ for CX Cep (Massey & Conti 1981), 10–20 $M_\odot$ for HD 211853 (Massey 1981). Considering that the latter systems consist of WN5, WN5 and WN6 respectively, compared to the WN7 in CQ Cep, the differences in derived mass are perhaps reasonable, since it is known that WN7 subgroup behaves differently from other subgroups in many respects (Moffat & Seggewiss 1980).

However, the energy distributions obtained by us at various phases do not show any evidence of change of slope of the Paschen continuum from conjunctions to

quadratures (Figs 1a and b), which could have been caused by an early-type companion.

Niemela (1980), analyzing the spectra at better dispersions (15 Å mm^{-1}) found evidence for absorption arising from the companion. Leung, Moffat & Seggewiss (1983) found that He I λ3888 probably represents line splitting due to companion. Stickland *et al.* (1984) also found such line splitting but only at one epoch, the velocity of the second component being almost constant. On the plates used in this study, the region $\sim \lambda$3888 is not exposed well enough. However, He I λ4471 definitely showed two components in 1951 (Bappu & Viswanadham, 1977). The measured radial velocities of one component show a variation similar to He I λ5876, which follows the motion of the WN component; the other component has a mean value of about -900 km s^{-1} with a large scatter. Obviously, this component can not represent the motion of the companion.

From the *UV* measurements of *P* Cyg profiles, Stickland *et al.* (1984) have derived the terminal velocity, the escape velocity and the ratio $M^*/R^* = 1.2\ M_\odot/R_\odot$. Accordingly, the radius can be either 18 $R_\odot$ (for the 20 $M_\odot$ WN component) or 38 $R_\odot$ (for the 46 $M_\odot$ WN component). The separation between the components in these two cases are $\sim 20\ R_\odot$ and 25 $R_\odot$ respectively, which conflicts with the sizes derived for stellar radii. Further, Underhill (1969) has pointed out that atmospheres of WR systems are extended to about 5 times the core radius. In this case, even for a smaller value of 10 $M_\odot$ for WN, the extension will be $\sim 45\ R_\odot$. Hence, irrespective of the method of light curve solution, the companion will be inside the stellar wind of the WN. It is also known that the WR atmospheres are generally optically thick for helium and hydrogen lines for $n < 10$ (Smith 1973). Hence these lines produced at the photosphere of the companion (which is completely embedded in the wind) will not be appreciably recognizable after passing through the thick atmosphere. To check this on spectra of medium dispersions is difficult, because the absorptions indicate the motion of WN itself. Any absorption due to the companion will move in the opposite direction, in case of helium lines, well within the 10 Å width of the emission profile. At phases close to 0.0 and 0.5, this absorption is expected to be superimposed on the emission profiles. At phase 0.25, this absorption would have moved away and at phase 0.75 it is likely to coincide with the violet wing of the emission profile. This can add to the total absorption at this phase making the effect easily recognizable, as was seen for He II λ4860 and λ6562 and to some extent for λ5410. Whether such an effect is present for λ4686 line is hard to decide not only because of its increased strength but also because of the building up of another strong emission of N III λ4640.

The radial velocity discrepancy curves generated with reference to N IV λ4058 show more positive values at all phases, reflecting mainly the shift in γ axes. Hence, it is difficult to judge the possibility of any contribution of opposite-moving absorption. The type of absorptions shown by He II $\lambda\lambda$4860, 6562 and 5410 have not been observed by Stickland (personal communication). This may also imply that these absorptions are probably of sporadic nature, although the observed amplitude differences (and almost circular orbit for only λ5410) appear constantly at all epochs.

In the absence of evidence from spectroscopic or spectrophotometric data, other than the only one high-dispersion measurement by Niemela (1980), we may assume that the companion is of spectral type O, contributing to absorption, if recognizable, only in He II and He I lines.

5.2 *Circumstellar Matter*

The radial velocity variations and flux variations may now be studied in order to understand the structure of the envelope surrounding the star. We use N IV λ4058 to represent the motion of the WN component for the following reasons: (1) The spectra clearly show that this line is free of any blends. (2) This line does not show asymmetry in line profile due to absorptions. (3) Its radial velocity curve gives an almost circular orbit, which is anticipated in case of such close binaries. (4) Its γ velocity has a value very close to the systemic velocity of other members of the Cepheus association (Stickland *et al.* 1984).

We may start with the nitrogen lines for understanding the WN atmosphere, since they are known to be formed in the WN atmosphere only and not in the companion. The flux variation of the Nv line shows eclipse effects, implying its formation in a region closer to the WN photosphere and, therefore, an approximate size of the line-emitting region may be calculated. We may also note that no eclipse effects are seen at phase 0.5, when the WN is between the observer and the O type star. Assuming that this line originates deep in the atmosphere we can think of a configuration of an eclipse of parts of this line-emitting sphere at the primary minimum. The depth of the eclipse is about 25 per cent and the duration of the eclipse is from phase 0.85 to 0.15. Then the radius of the line-emitting region will be about 10 $R_\odot$.

From the variation of the line profile we see that absorption and emission are moving together so as to leave the profile unchanged. This further indicates that the decrease in flux at phase 0.0 corresponds to an eclipse effect only. The radial velocity curves of this line show an interesting phenomenon; these curves are identical but for a shift in γ axes. If we assume that this line originated in a region close to the photosphere, it should follow the characteristics of N IV λ4058, *i.e.*, γ axis should have been -65 km s^{-1}. But because of the associated absorption there can be a positive shift of γ axis. It may be noticed that when we combine the effect of emission and absorption the net value of γ will be -56 km s^{-1}. This would imply that the redshift of γ axis is due to the associated absorption only. However, it is not possible to verify whether this effect exists for all other lines with absorptions or whether it is just a coincidence in case of N v λ4603.

The behaviour of helium lines has already been discussed in the previous section. Here, the shift in γ axes may be a consequence of the absorption arising in the WN itself (like N v λ4603) or because of the absorption due to the companion. A situation like this, of two absorption features moving in opposite directions, can reduce the total flux also at phases 0.25 and 0.75. At phase 0.75 both absorptions add to the violet wing of the profile so that the measured flux will be still smaller. This is partly true, because on some occasions at phases ~ 0.75 the flux was too small to make any meaningful measurements. But this cannot totally explain the observed flux increase at phases 0.0 and 0.5.

The absence of eclipse effects for all lines other than N v λ4603 demands that their line-emitting regions will have to be larger than 10 $R_\odot$ (the value of the same for N v λ4603). This also sets a limit on the size of the companion at ~ 10 $R_\odot$. As discussed in the previous section the companion definitely sweeps through the WN stellar wind, thus partly occulting the wind during quadratures, while at minima the entire line-emitting region is visible. This geometrical effect will cause an apparent increase of flux at minima. This scenario is likely to be more plausible specially in case of CQ Cep,

because in V444 Cyg the companion is larger and all the lines show eclipse effects.

Thus it appears that in case of helium lines absorption and geometric effects cause the observed flux variation while for other lines it is mainly the geometric effect.

6. Discussion

Various models have been put forward to explain the line flux variation by the earlier investigators. The common-envelope model proposed by Bappu (1951a) explains the occultation effects, but assumes that He I lines originate deeper in the envelope compared to He II, which contradicts the velocity *versus* excitation potential (EP) relation derived from *UV* line profiles (Stickland *et al.* 1984). Sahade proposed a stream from WN towards the companion to be responsible for enhancement of He II λ4686 (*cf.* Hack & Struve 1970). Leung, Moffat & Seggewiss (1983) provided the light-curve solutions with a mass ratio of $q = 0.75$ and explained the behaviour of some lines at phase 0.8 by assuming that the line-emitting material has a maximum velocity towards the observer at that phase. The latest model by Stickland *et al.* (1984) takes into account the difficulties encountered in fitting a simple model, and provides a hot zone between the two stars and an enhanced outflow.

6.1 *The Roche Surface*

The only emission line which shows eclipse effects is N V λ4603. If this is used for estimating the size of the line-emitting region, the size will be just equal to the inner Roche surface calculated from tables of Plavec & Kratochvil (1964). The use of these tables needs many assumptions about the components. Considering the large wind velocities of the WN component and the large extension of the atmosphere, this picture of the Roche surfaces is probably not applicable. Schuerman (1972) introduced these effects into calculations and showed that the deformation of the Roche surfaces was applicable to massive X-ray binaries. Zorec & Niemela (1980a and b) considered the radiation pressure from both components and applied to the case of V444 Cyg (*cf.* Sahade & Wood 1980). Vanbeveren (1977) considered X-ray heating, deviations from synchronous rotation and a different rate of synchronization for the two components. From all these studies, it is clear that the tables of Plavec & Kratochvil (1964) are not applicable for systems like CQ Cep. The Roche surface will extend towards the companion with lower radiation pressure, making the distribution highly asymmetric and distorting the spherical shape of the components into ellipsoids.

A sample Roche surface from Vanbeveren (1977) can be chosen for the purpose of determining asymmetries. Only hemispheres are considered for determining the ratios of line-emitting material at four phases, because it is established that generally the helium lines (considered in this work) are optically thick (Smith 1973). The ratios at phases 0.0, 0.25, 0.5 and 0.75 are 9.0:6.3:7.6:6.3 respectively. Thus at phase 0.0 the flux can be the highest, although the companion occults a small portion of the atmosphere. This kind of a flux distribution is seen for He II λ4686. For N IV λ4058 and other lines the fluxes at 0.0 and 0.5 are almost equal. This may imply that their distribution is not as asymmetric as that of λ4686. The optical thinness of N IV lines and N III lines also may be partly responsible for this.

Kuhi (1968) suggested a hot zone between the two components of V444 Cyg because the eclipse effects were seen for all emission lines. The distribution of emitting material, in such a situation shows concentration towards the inner Lagrangian point. This will be recognizable in line profiles as is seen for He II λ4686 in V444 Cyg as a hump moving with phase (Ganesh, Bappu & Natarajan 1967). Similar observations have been done for C III λ5696 in case of θ Mus (Moffat & Seggewiss 1977). No such line-profile change is noticeable in CQ Cep. Therefore, either the inner Lagrangian point or Roche surface cannot explain the behaviour of emission line fluxes.

6.2 *Inferences from UV and IR Studies*

Hackwell, Gehrz & Smith (1974) were the first to detect the IR excess of CQ Cep. They also showed that for this system only a free-free emission can be fitted and not a blackbody fit, as was possible for other WR systems. Stickland *et al.* (1984) obtained the IR light curves and showed that the amplitude of the light curve decreases towards IR wavelengths. Hence the presence of a 'third source' could be recognized. The asymmetry in the distribution of a 'third source' is also similar to that of other emission lines.

The fluxes for different emission lines also have been measured by Stickland *et al.* (1984) in the *UV*. The behaviour is similar to the variation seen in this work for emission lines in the optical. The emissions in *UV* and optical thus show enhancement of flux at phases near 0.0 and 0.5. Stickland *et al.* have also shown that there is one unidentified line, whose flux variation is similar to that of N V λ4603, showing eclipse effects. The equivalent widths of some absorptions also have been measured. They have larger values at quadratures.

6.3 *Peculiarities of some Emission Lines*

We notice that the emission lines in general show enhancement at phases $\sim$ 0.0 and 0.5. However, He II λ4686 has larger flux at $\sim$ 0.0 and the increase is sudden. N III λ4640 does not show much variation. The radial velocity curves of these two lines have smaller values of amplitude compared to any other line. Taking N IV λ4058 as representative of the WN motion, the radial-velocity discrepancy curves for all other emission lines can be generated. These curves reflect only the differences in γ velocities and amplitudes; in general, they all show small variation through the phase, the effect being larger for lines giving eccentric orbit solutions. In these curves again the difference of λ4686 and λ4640 lines shows up: they show larger discrepancies. This may be qualitatively explained by assuming that the emitting material is distributed over a larger extent in the atmosphere. This reduces the amplitude of radial velocity curve and increases the strength of the line. The classification into WN7 itself implies the large strengths of these two lines.

In the case of V444 Cyg, Kuhi (1968) observed that λ4686 and λ4640 were brightest immediately after the secondary eclipse. The eclipse depths also were different compared to other lines of same ionization.

It is important to note that all the He I lines have violet absorption edges produced

throughout the cycle. The velocities associated are also quite high and they follow a velocity *vs* EP relation (Stickland *et al.* 1984). This clearly confirms that they originate in the outermost regions of the extended atmosphere and are probably undisturbed by the presence of the companion although the structural changes of some lines like λ6678 may be attributed to the companion.

6.4 *Sporadic Events*

A sporadic brightening of the order of 0.03 mag was noticed by Hiltner (1950). Later Kartasheva (1976) reported variations up to 0.1 mag in 10 months. Both these observations were for the continuum only. However, in 1950, Hiltner also noticed a sudden change in the strength of He II λ4686. It is possible that we have a similar situation in 1982, when a sudden increase in flux at phase $\sim$ 0.9 was recorded. Excepting this sporadic strengthening, the behaviour of λ4686 is similar to other lines. The peculiar behaviour of He I lines has been already discussed: λ4471 showed splitting in Hiltner's plates taken in 1943, and in Bappu's collection of 1952. Similar splitting of λ3888 was noticed in 1978 (Leung, Moffat & Seggewiss 1983). Therefore, it is likely that some transient phenomena like an enhancement of mass loss (Stickland *et al.*, 1984) were responsible for such line splitting. High dispersion spectra can reveal these aspects and the possible effect due to the companion.

7. Comparison with V444 Cyg

V444 Cyg (period 4.2 days) is the only binary with more detailed studies on the line profiles and radial velocities. Here the O-type companion is detected by its absorption spectrum and, in fact, is larger and more massive of the two. Kuhi (1968) studied the secondary eclipse so that the O-type star may be treated as an occulting disc passing in front of the WN atmosphere. He mentions the highly individualistic behaviour of lines. The difference with reference to λ4640 and λ4686 has already been mentioned. The line profiles have been studied by Ganesh, Bappu & Natarajan (1967). N IV λ4058 shows symmetric profiles, but appears to be broader at quadrature than at conjunctions. Such profile changes are present in CQ Cep also on a very small scale (Bappu & Viswanadham 1977). In the case of V444 Cyg, the profile of He II λ4686 shows a superimposed hump, as discussed in Section 6.1.

Following the stratification of CQ Cep we may try to interpret the eclipse observations of Kuhi (1968). N V lines being formed closest to the photosphere should show deepest eclipses. This is only partly true, because the deepest eclipse is that of N IV λ7112.

The Roche surface has been calculated by Niemela taking into account the stellar wind (*cf.* Sahade & Wood 1980). It may be noticed that at phase 0.5 when the O star is in front, the line-emitting region is still visible. A larger portion of the line-emitting region will be covered by the O star just before (or after, depending on *i*) phase 0.5. This may partly explain the shift of some eclipses from phase 0.5.

Since all the emissions are definitely showing eclipses, it appears that their line-emitting regions are of comparable size to the companion *i.e.* $\sim$ 10 $R_\odot$. Thus there is a large difference in sizes of envelopes around the WN component in CQ Cep and V444

Cyg; For CQ Cep, 10 $R_\odot$ was the lower limit. Observing the difference in masses, absolute magnitudes, ionization structure and abundances between WN5 and WN7 (Moffat & Seggewiss 1980), this change in the size of wind and atmosphere is also probably real.

8. Conclusions

This spectrophotometric study of the shortest period Wolf-Rayet binary clearly shows the complicated structure of WN7 atmosphere. Of the many lines available in the optical region for study, only N v λ4603 shows eclipse effects. The flux variations of other emission lines appear to differ from the continuum variations. They can be explained by Roche surfaces taking into account the strong wind of the WN7 component. N iv λ4058 represents the true motion of the WN7 component and its flux variations appear to be influenced by the geometric effects of wind-dominated Roche surface.

Any signature of the companion is not detectable. The emission lines generally show a positive shift for the motion of the centre of mass (γ axis). This may be due to the strong wind characteristics and, in case of helium lines, possible absorptions from the companion. The optical thickness of this wind to the helium lines is also probably responsible for the non-detection of any line from the companion, which, according to light-curve solutions, is deeply embedded in the wind. These strong winds further prevent the application of classical, gravity-dominated Roche surfaces. Studies of high dispersion spectra may reveal weak spectral lines of companion at phases 0.25 and 0.75.

The behaviour of the strongest lines in the optical spectrum, N iii λ4640 and He ii λ4686 Å differs from all other emission lines in both the radial-velocity variations as well as flux variations. Sporadic events like brightening of the spectral lines, and line splitting corresponding to enhanced mass loss appear to occur occasionally.

A comparison with the only well-studied binary V444 Cyg shows a larger extent of the atmosphere, which probably is due to the inherent differences between the two subgroups WN5 and WN7.

Acknowledgements

I gratefully acknowledge late Professor M. K. V. Bappu, under whose guidance I began these studies. A critical reading of the manuscript by Drs D. J. Stickland and R. Rajamohan was immensely helpful. I acknowledge useful discussions with Professors J. C. Bhattacharyya, R. Koch, C. de Loore and K. D. Abhyankar. Valuable suggestions by Drs G. S. D. Babu, G. C. Kilambi, N. K. Rao, C. Sivaram, M. Parthasarathy and D. C. V. Mallik, were very helpful during the analysis. I thank Mr M. N. M. Rao for help in the reduction of the data on TDC 316 computer. I also thank the referees for useful suggestions.

References

Bappu, M. K. V. 1951a, PhD *Thesis*, Harvard Univ.
Bappu, M. K. V. 1951b, *Astr. J.*, **56**, 120.

Bappu, M. K. V. 1952, *Astr. J.*, **57,** 6.
Bappu, M. K. V. , Sinvhal, S. D. 1955, *Astr. J.*, **60,** 152.
Bappu, M. K. V., Sinvhal, S. D. 1959, *Observatory*, **79,** 140.
Bappu, M. K. V. 1973, in *IAU Symp.* 49*: Wolf-Rayet and High-Temperature Stars*, Eds M. K. V. Bappu & J. Sahade, D. Reidel, Dordrecht, p. 59.
Bappu, M. K. V. 1977, *Kodaikanal Obs. Bull. Ser. A*, **2,** 64.
Bappu, M. K. V., Viswanadham, P. 1977, *Kodaikanal Obs. Bull. Ser. A*, **2,** 89.
Breger, M. 1976, *Astrophys. J. Suppl. Ser.*, **32,** 1.
Cherepashchuk, A. M., Khaliullin, Kh. F. 1976, *Soviet Astr.*, **19,** 727.
Ganesh, K. S., Bappu, M. K. V., Natarajan, V. 1967, *Kodaikanal Obs. Bull. Ser.* A, No. 184, 93.
Giridhar, S. 1978, *Kodaikanal Obs. Bull. Ser. A*, **2,** 164.
Hack, M., Struve, O. 1970, in *Stellar Spectroscopy: Peculiar Stars*, Osser. Astr. Trieste, p. 129.
Hackwell, J. A., Gehrz, R. D., Smith, J. R. 1974, *Astrophys. J.*, **192,** 383.
Hayes, D. S. 1970, *Astrophys. J.*, **159,** 165.
Hiltner, W. A. 1950, *Astrophys. J.*, **112,** 477.
Hua, C. T., Woo, J. O., Nguyen, H. D. 1982, *Astr. Astrophys. Suppl. Ser.*, **53,** 407.
Kartasheva, T. A. 1976, *Soviet Astr. Lett.*, **2,** 197.
Khaliullin, Kh. F. 1973, *Soviet Astr.*, **16,** 636.
Kuhi, L. V. 1966, *Astrophys. J.*, **143,** 753.
Kuhi, L. V. 1968, *Astrophys. J.*, **152,** 89.
Leung, K. C., Moffat, A. F. J., Seggewiss, W. 1983, *Astrophys. J.*, **265,** 961.
Massey, P. 1981, *Astrophys. J.*, **244,** 157.
Massey, P., Conti, P. S. 1981, *Astrophys. J.*, **244,** 169.
Moffat, A. F. J., Seggewiss, W. 1977, *Astr. Astrophys.*, **54,** 607.
Moffat, A. F. J., Seggewiss, W. 1980, in *IAU Symp.* 83*: Mass-loss and Evolution of* O *type stars*, Eds P. S. Conti & C. W. H. de Loore, D. Reidel, Dordrecht, p. 447.
Niemela, V. S. 1980, in IAU Symp. 88: *Close Binary Stars: Observations and Interpretations*, Eds M. J. Plavec, D. M. Popper & R. K. Ulrich, D. Reidel, Dordrecht, p. 177.
Plavec, M., Kratochvil, P. 1964, *Bull. astr. Inst. Csl.*, **15,** 165.
Sahade, J., Wood, F. B. 1978, in *Interacting Binary Stars*, Pergamon Press, p. 101.
Schuerman, D. W. 1972, *Astrophys. Space Sci.*, **19,** 351.
Semeniuk, I. 1968, *Acta. Astr.*, **18,** 313.
Smith, L.F. 1973, in *IAU Symp.* 49*: Wolf-Rayet and High-Temperature Stars*, Eds M. K. V. Bappu & J. Sahade, D. Reidel, Dordrecht, p.15.
Stickland, D. J., Bromage, G. E., Budding, E., Burton, W. M., Howrath, I. D., Jameson, R., Scherrington, M. R., Willis, A. J. 1984, *Astr. Astrophys.*, **134,** 45.
Underhill, A. B., 1969, in *Mass-loss from Stars*, Ed. M. Hack, D. Reidel, Dordrecht, p. 17.
Vanbeveren, D. 1977, *Astr. Astrophys.*, **54,** 877.
van der Hucht, K. A., Conti, P. S., Lundström, I., Stenholm, B. 1981, *Space Sci. Rev.*, **28,** 227.
Walker, E. N., Lloyd, C., Pike, C. D., Stickland, D. J., Zuiderwijk, E. J. 1983, *Astr. Astrophys.*, **128,** 394.
Zorec, J., Niemela, V. 1980a, *C. R. Acad. Sci. Paris*, **290,** Ser. B, 67.
Zorec, J., Niemela, V. S. 1980b, *C. R. Acad. Sci. Paris*, **290,** Ser. B, 95.